Computational Materials Science xxx (xxxx) 110461

Contents lists available at ScienceDirect

Computational Materials Science

journal homepage: www.elsevier.com/locate/commatsci

# Formation energies of $\theta$-$Al_2Cu$ phase and precursor Al-Cu compounds: Importance of on-site Coulomb repulsion

M. Souissi [a,*], C.M. Fang [a], R. Sahara [b], Z. Fan [a]

[a] BCAST, Brunel University London, Uxbridge, Middlesex, UB8 3PH, UK
[b] Research Center for Structural Materials, National Institute for Materials Science, 1-2-1 Sengen, Tsukuba, Ibaraki, 305-0047, Japan

ARTICLE INFO

*Keywords:*
Formation energy
Coulomb on-site repulsion
DFT + U
$Al_2Cu$ phases
Al-Cu alloys

ABSTRACT

We investigated the relative stability and structural properties of Al-Cu intermetallic compounds using the density-functional theory (DFT) with different approximations. We reveal the importance of the on-site Coulomb repulsion of Cu *3d* electrons on the energetics and structural properties of Al-Cu compounds of free-electron nature. The finite-temperature effect was included by accounting for the vibrational free energy within the Debye model. The present study shows that $\theta$-$Al_2Cu$ is the ground state phase, agreeing with the experimental observations in the literature. The DFT + U approach could be useful to predict accurate formation energies of other Cu-containing precipitates in high-strength Al-alloys.

## 1. Introduction

Substitutional precipitate hardening is the principal mechanism to strengthen aluminum alloys [1]. In aluminium-copper (Al-Cu) alloys, for example, Cu clustering and precipitation have been extensively studied for many years, owing to the advances of experimental and computational techniques [2]. The development of refine precipitate observations and advanced modeling approaches has significantly contributed to a better understanding of the microscopic mechanisms of early precipitation stages [3,4].

Thermally activated pre-nucleation stages and metastable precipitates are formed during aging after Cu solute clustering, later by the formation of different Cu layers. As discovered 82 years ago by X-ray observations [5], Guinier-Preston zones, GPZs (GPI), were observed as series of streaks parallel to the (1 0 0) planes of the crystal, with various lengths up to 4 nm. Then, $\theta''$-$Al_3Cu$ structures, GPII zones, form when three Al layers come together in between two Cu layers. It is commonly accepted that the Cu precipitation occurs in the following sequence of metastable phases: Super Saturated Solid Solution (SSSS) → Solute clusters → GPI → GPII → $\theta''$-$Al_3Cu$ → $\theta'$-$Al_2Cu$ → $\theta$-$Al_2Cu$. This sequence is found in most of the textbooks [6–8]. Although the precipitation in binary Al-Cu alloys is well documented, comprehensive knowledge of the precipitation mechanism and the transition between nucleation stages is still lacking.

Theoretical calculations can provide substantial information "on what is really going on" to describe the morphological sequence of GPZs. Wang et al. [9] have studied the energetics of series of Al-Cu superlattices using the Local Density Approximation (LDA) approach. They have shown that stability increases with Cu content increase. The formation sequence of GPZs in Al-Cu alloys resemble an accumulation of Cu atoms via agglomeration of Cu plates. Previous *ab initio* studies showed that the formation energy of $\theta$-$Al_2Cu$ phase is higher than that of the $\theta'$-$Al_2Cu$ phase [9], indicating that the $\theta'$-$Al_2Cu$ is more stable than $\theta$-$Al_2Cu$ phase [9]. This contradicts the experimental observations, where the $\theta$-$Al_2Cu$ phase is the ground state phase and is more stable than the $\theta'$-$Al_2Cu$ phase [10].

Here we show that the formation energies of the $\theta$-$Al_2Cu$ phase and Al-Cu compounds are corrected by taking into account the Cu on-site *3d* Coulomb repulsion using the DFT + U approach. A ground state formation energy was obtained for the $\theta$-$Al_2Cu$ phase. After adding the contribution of vibrational free energy, Gibbs free energy showed a stability gain for the $\theta$-$Al_2Cu$ phase over $\theta'$-$Al_2Cu$ phase at high temperatures. Our computed results are in line with the experiment. The present method could be able to predict accurate formation energies of precipitates containing Cu.

## 2. Method

### 2.1. DFT + U approach and adopted Hubbard model

We have performed total energy calculations using density functional theory (DFT) and DFT + U (U is Hubbard term) as implemented

* Corresponding author at: BCAST, Brunel University London, Kingston Lane, Uxbridge, UB8 3PH, UK.
*E-mail address:* Maaouia.Souissi@brunel.ac.uk (M. Souissi).

https://doi.org/10.1016/j.commatsci.2021.110461
Received 2 November 2020; Received in revised form 8 February 2021; Accepted 20 March 2021
0927-0256/

in the Vienna *ab initio* Simulation Package [11,12]. We employed the projected augmented wave (PAW) potentials and the generalized gradient approximation (GGA) of Perdew-Burke-Ernzerhof (PBE) for exchange–correlation [13]. The electronic configurations are for Cu:[Ar]$3d^{10}4p^1$ and Al:[Ne]$3s^23p^1$, respectively. At first, 3 × 3 × 3 face-centered cubic (fcc) unit cell (108 atoms), 2 × 2 × 2 fcc unit cell (32 atoms) and 2 × 2 × 3 fcc unit cell (48 atoms) with one single Cu atom were selected for computing the dilute solution, then 2 × 2 × 2 supercell (32 atoms) was considered for the nucleation of GPZ precipitates up to $\theta''$-$Al_3Cu$ formation, and Al-Cu compounds in addition to the conventional supercells of $\theta'$-$Al_2Cu$ and $\theta$-$Al_2Cu$. The Methfessel-Paxton method was used to relax both the lattice parameters and coordinates of atoms to reach equilibrium. The cutoff energies for the plane-wave basis set and the representation of the augmentation charges are [illegible] and 700 eV, respectively, for all cells. The calculations were s[illegible] to converge when total energy researched less than $10^{-5}$ eV per atom and interatomic forces less than $10^{-4}$ eV/A, respectively.

While standard DFT has successfully predicted the structures properties of a wide range of materials, it fails to estimate certain other properties, such as the formation energies of Al-Cu phases in the present study. [illegible]ason behind this arises from the electron–electron interaction at [illegible]zed orbitals [14]. Many efforts have been proposed to describe the strongly correlated electron systems correctly. One is the DFT + U method [15], which introduces a repulsion between the localized electrons, where a repulsive term referred to as the Hubbard U is introduced. The physical effect of the U term is to shift the localized orbitals, which increases the gap between the filled and the empty states, removing the unphysical self-interaction to get the proper ground state and correct the bandgap of the system.

In this study, we employed several density-functionals, including the standard GGA and GGA + U to describe the Al-Cu precipitates. We used the DFT + U approach to correct standard GGA exchange–correlation by including the on-site Coulomb repulsion in the *3d* localized bands based on the Mott-Hubbard model approach [16,17]. An energy expression based on the on-site density matrix $\rho_{ij}$ of the Cu 3*d* electrons can be given as,

$$E_{\mathrm{GGA-PBE+U}} = E_{\mathrm{GGA-PBE}} + \frac{(\mathrm{U}-\mathrm{J})}{2}\sum\left[\sum_j \rho_{jj} - \sum_{j,i}\rho_{ji}\rho_{ij}\right] \quad (1)$$

where U is the averaged Hubbard parameter, and J represents the screened exchange energy. The Hubbard U value used is crucial for the formation energy accuracy derived in this work. A concise formalism of the DFT + U concept is found in [14].

The formation energy per Cu atom of Al-Cu precipitates and compounds at 0 K is derived from the following expression,

$$\Delta E\left(\mathrm{Al}_n\mathrm{Cu}_m\right)/\mathrm{Cuatom} = [E\left(\mathrm{Al}_n\mathrm{Cu}_m\right) - nE\left(\mathrm{Al}\right) - mE\left(\mathrm{Cu}\right)]/m \quad (2)$$

where $E(\mathrm{Al}_n\mathrm{Cu}_m)$ is the total energy of the Al-Cu system, $E$(Al) and $E$(Cu) are the elemental total energies of reference for Al and Cu. $n$ and $m$ represent the number of Al and Cu atoms, respectively.

### 2.2. Vibrational entropy [illegible]ution and Debye model

A substantial effect on the stability of $\theta$-$Al_2Cu$ phase could be obtained by adding the vibrational contribution to 0 K formation energy. In this section, we show that the phase stability of the Al-Cu precipitates can be further enhanced by accounting for the Gibbs free energy, whereby the lattice vibration of the compounds is included in the calculations of total free energy within the Debye model [18,19].

The free energy of an Al-Cu structure, $G(T)$, is obtained by adding the temperature dependent vibrational free energy, $G_{\mathrm{Debye}}(T)$, to the *ab initio* computed formation energy at 0 K, $\Delta E$,

$$G(T) = \Delta E + G_{\mathrm{Debye}}(T) \quad (3)$$

where $T$ is the absolute temperature. The Debye vibrational free energy is computed with

$$G_{\mathrm{Debye}}(T) = \frac{9}{8}k_B T_D + k_B T \times \left[3\ln\left(1 - e^{-\frac{T_D}{T}}\right) - \mathrm{D}_3\left(\frac{T_D}{T}\right)\right] \quad (4)$$

where $k_B$ is Boltzmann's constant, $T_D$ is the Debye temperature adopted from [20], and $\mathrm{D}_3\left(\frac{T_D}{T}\right)$ is the Debye integral defined as,

$$\mathrm{D}_3\left(\frac{T_D}{T}\right) = \frac{3}{T_D^3}T^3\int_0^{T_D/T}\frac{t^3}{e^t - 1}dt \quad (5)$$

where $t = \hbar v_s\left|\vec{\omega}\right|/(k_B T)$, $v_s$ is the velocity of the sound wave and $\left|\vec{\omega}\right|$ is the wave vector.

In Eq. (4), the first term on the right-hand side denotes the zero-point vibrational contribution and the second indicates the temperature-dependent vibrational contribution. The formation free energy will be given as,

$$\Delta G_f(T)\left[\mathrm{Al}_{1-x}\mathrm{Cu}_x\right] = G(T)\left[\mathrm{Al}_{1-x}\mathrm{Cu}_x\right] - \{(1-x)G(T)\left[\mathrm{Al}_{1-x}\right] + xG(T)\left[\mathrm{Cu}_x\right]\} \quad (6)$$

where $x$ [illegible] $/(n + m)$. The thermodynamically favored structure is determi[illegible] minimizing $\Delta G_f(T)$. In our calculations, we have neglected the effects of thermal volume expansion. Also, since the Al-Cu structures are ordered, the configurational entropy term has not been accounted for.

### 2.3. Hubbard model validation and determination of U term

To determine the pr[illegible]per value of Hubbard term U, we looked first at the experimental Cu 3d photoemission peaks and we generated Cu 3d local density of states using the DFT + U[illegible]d for comparison. Fig. 1 shows the X-ray photoemission spectru[illegible]S) (circles symbols with line) together with the ultraviolet photoemission spectrum (UPS) (solid line) of the Cu 3d photoemission peaks of the valence band [21], [illegible] ted against ab initio [illegible]y of states of Cu 3d orbital derived from standard density functional PBE-GGA without (dashed line) and with Hubbard U correction (U = 4 eV) (solid red line), of pure Cu (Fig. 1b), the dilute solution ($Al_{107}Cu$) (Fig. 1c), $\theta''$-$Al_3Cu$ ((Fig. 1d), $\theta'$-$Al_2Cu$ (Fig. 1e), and $\theta$-$Al_2Cu$ phases (Fig. 1f). The Fermi level is at 0 eV.

In principle, XPS or UPS spectrums can be compared to the local density of states (LDOS) obtained from DFT bulk-calculations [22]. However, the comparison of the calculated LDOS to the experimental spectra is a subtle task, depending on the adjustment of experimental broadening and the consideration of different photoionization cross-sections of the other atoms and orbitals. In our case, Cu 3d [illegible]bital has a dominant contribution over the Cu 1s state on the Cu-Cu binding. Therefore, the experimental spectra and bulk LDOS calculations may match well in the *d*-band region [23]. Also, we expect the Cu-Cu binding to be mainly dependent on valence electrons, and it will not be affected much by the inclusion of Cu core electrons.

From the XPS and UPS measurements, the highest peaks are locate[illegible] at –3.2 eV (XPS) and –2.4 eV (UPS) (Fig. 1a). Whereas the highest 3d peaks derived from our calculations are located at –1.66 eV (PBE-GGA) and –2.3 eV (PBE + U). The density of states derived from the standard approach is located at higher energy interval than the ones obtained by

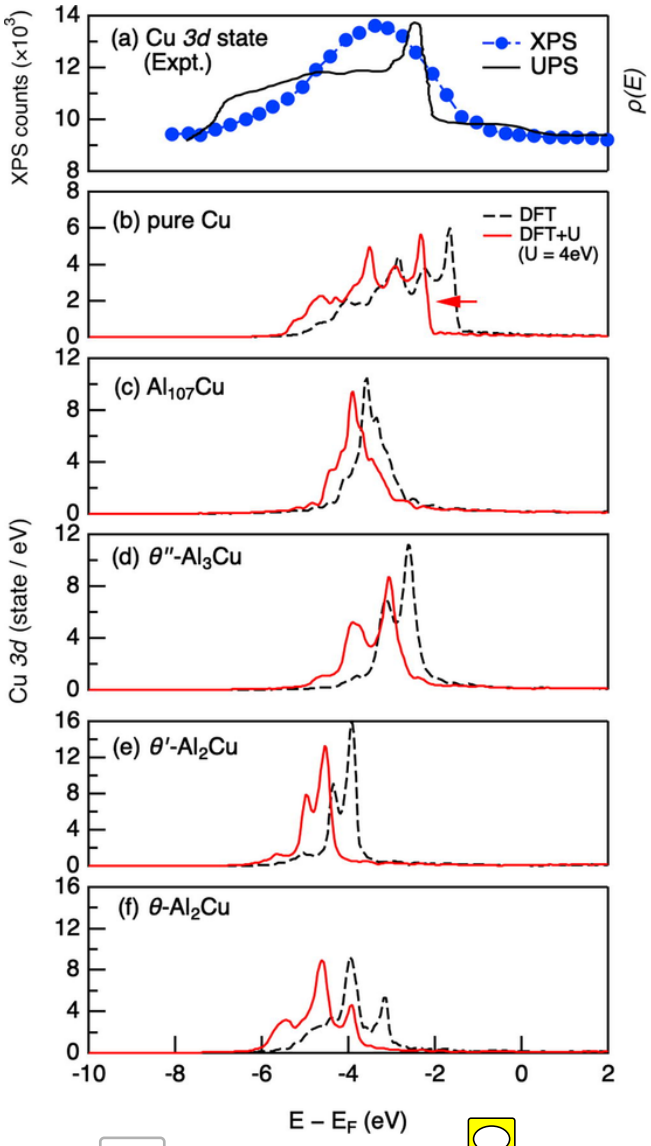


**Fig. 1.** (a) V and photoelectron spectrum (XPS) produced by exposure of Cu to Mg showing a peak due to the *3d* bands of Cu e curve obtained from ultraviolet photoelectron spectroscopy (UPS) is l on the same graph for comparison. Peaks are located at –3.2 eV (XP d –2.4 eV (UPS). *Ab initio* density of states of Cu 3d derived from standard density functional PBE-GGA without (dashed line ith Hubbard U correction term (U = 4 eV) (solid red line) for (b) pure Cu, where the highest *3d* pea s are located at –1.66 eV (PBE-GGA) and –2.3 eV (PBE + U), (c) the dilute solution ($Al_{107}Cu$), (d) $\theta''$-$Al_3Cu$, (e) $\theta'\theta'$-$Al_2Cu$, and (f) $\theta$-$Al_2Cu$ phases. The Fermi level is normalized at 0 eV.

the XPS or UPS. An energy shift toward lower energies of the PBE + U, with U = 4 eV, has corrected this mismatch, and for pure Cu, we have noticed a clear matching of the PBE + U highest peak with the highest peak measured by the UPS. Moreover, U = 4 eV has been widely used for CuO system [24]. Thus, we have adopted the same U value in the calculations of formation enthalpies of other Al-Cu phases. For the $Al_{107}Cu$ structure, the electron density has a single main peak for both DFT and DFT + U, where the peak height dropped by ~ 11%, and the energy shift between the results of DFT and those of DFT + U was ~ –0.346 eV. On the other hand, for the $\theta''\theta''$-$Al_3Cu$ phase, we noticed that the phase has two prominent electron density peaks. The first has shifted by –0.450 eV and dropped by ~26% and the second peak shifted by –0.764 eV with a height loss of ~33%. The lower energy shitting calculated for the $\theta''\theta''$-$Al_3Cu$ phase compared to the dilute solution represented by $Al_{107}Cu$ highlights the starting of Cu clustering through Cu-Cu nearest-neighbor interactions. For $\theta'\theta'$-$Al_2Cu$ phase, we observed two sharp electron density peaks. The first peak is higher than the second. A premature third peak is also captured. We expect the sharp peaks calculated for the $\theta'\theta'$-$Al_2Cu$ phase to be related to the metastability of the structure. Finally, we observed three main density peaks for $\theta$-$Al_2Cu$. The first two have a height loss of ~9% and 3%, with ~–0.769 eV and ~ –0.678 eV energy shifts. The third peak has gained 37% in height, with ~ –0.571 eV energy shifting. This peak, in particular, which we believe was born in the $\theta'\theta'$-$Al_2Cu$ phase, becomes bigger in the $\theta$-$Al_2Cu$ phase, indicating its thermodynamic stability. Overall, one clearly can see, the larger energy broadening calculated for $\theta$-$Al_2Cu$ phase, as compared to other phases, where the already well-established three electron density peaks show the high stability of the phase.

## 3. Results and discussion

### 3.1. Formation energy at 0 K

We first performed the energy dependence on U values for $\theta$- and $\theta'\theta'$-$Al_2Cu$ phases. Fig. 2 shows the variation of formation energy difference, [$\theta'\Delta E[\theta$-$Al_2Cu] – $\Delta E[\theta'$-$Al_2Cu]$ (meV/atom), between $\theta$- and $\theta'$ phases as a function of U used in the DFT + U approach. The calculations reveal that the formation energy difference is ~ –3.84 meV U = 4 eV and $\theta$-$Al_2Cu$ phase is the most stable phase, and this eement with the experiment [25].

Here we rep r results about the formation energy of $Al_{1-x}Cu_x$ configurations, calculated per Cu atom as a function of Cu atomic fraction, *x*. Fig. 3 illustrates the main crystal structures and configurations computed in the present study. The lattice structures of previously studied Al-Cu compounds and phases (Fig. 3a), the non-bulk $\theta''\theta''$-$Al_3Cu$ phase embedded into Al-matrix (Fig. 3b) and lowest energy configurations forming monolayer GPZs, and showing eight stages of Cu clustering (case of 2 × 2 × 2 fcc unit cell with 32 atoms) (Fig. 3c).

Fig. 4 shows the formation energy as a function of Cu content, *x*, of dilute solution represented by $Al_{107}Cu$, $Al_{47}Cu$, and $Al_{31}Cu$ structures, using 3 × 3 × 3 supercell (108 atoms), 2 × 2 × 3 supercell (48 atoms) and 2 × 2 × 2 supercell (32 atoms), respectively (Fig. 4a), GP

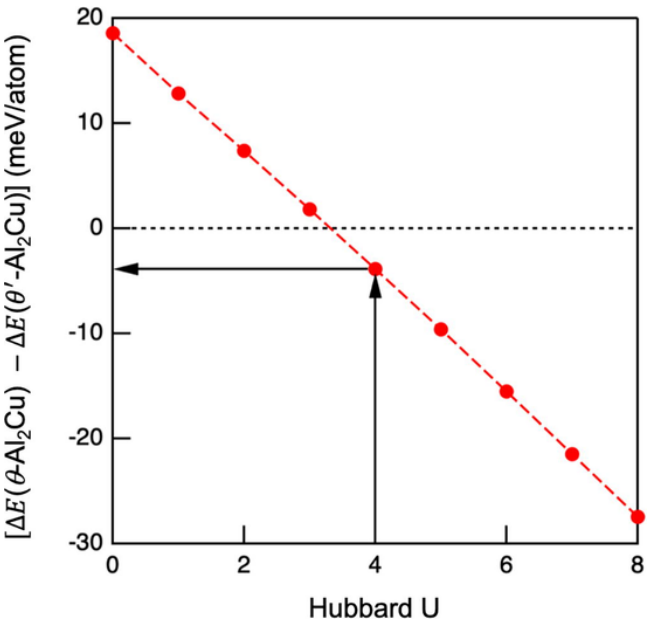


**Fig. 2.** Formation energy difference, [$\Delta E(\theta$-$Al_2Cu)$ – $\Delta E(\theta'$-$Al_2Cu)$] (meV/atom), between $\theta$- and $\theta'$-$Al_2Cu$ phases as a function of Hubbard U term used in DFT + U approach.

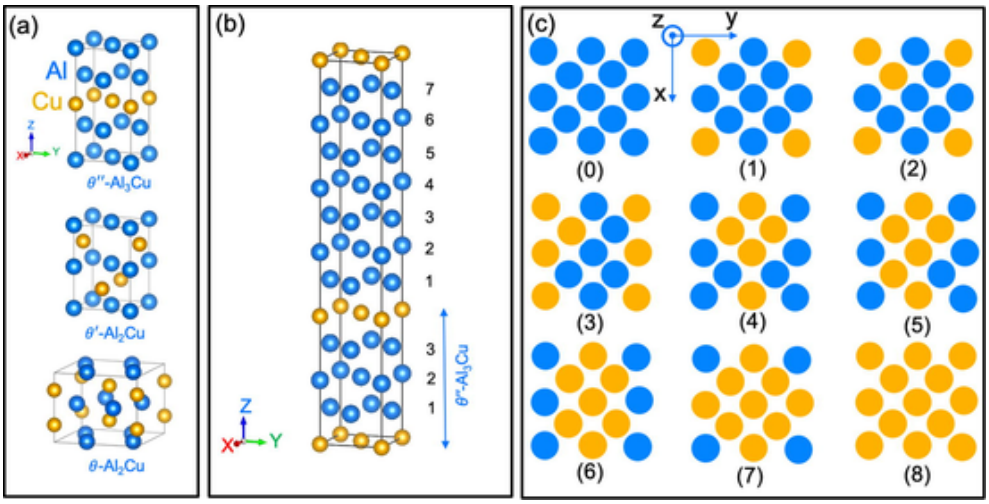


**Fig. 3.** (a) Structures of conventional cells of $\prime\prime\theta''$-$Al_3Cu$, $\prime\theta'$-$Al_2Cu$ and $\theta$-$Al_2Cu$ phases, and (b) currently selected model to compute formation of monolayer GPZs and embedded $\prime\prime\theta''$-$Al_3Cu$ isolated by 7 Al layers, (c) [illegible]ergy configuration derived from 2 × 2 × 2 fcc unit cell (32 atoms), showing the preference of Cu-Cu nearest-neighbor bondings.

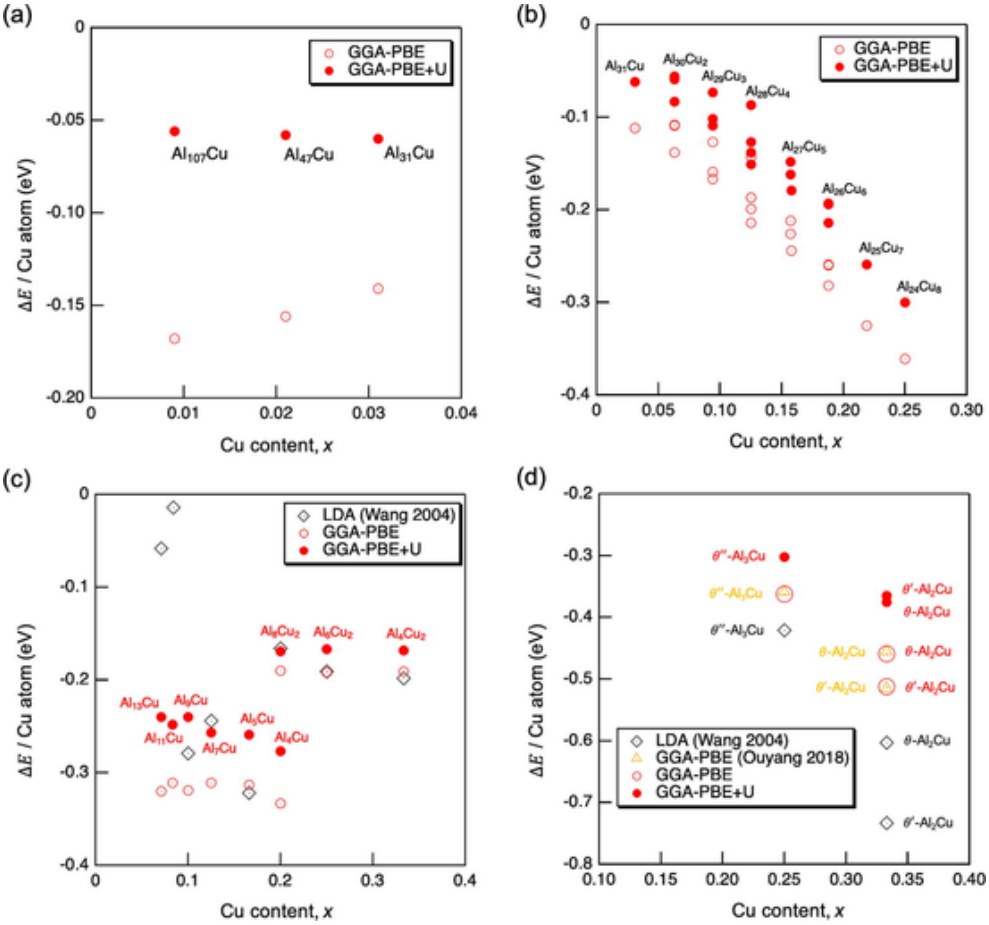


**Fig. 4.** Formation energy as a function of Cu content, $x$, of (a) dilute solution ($Al_{107}Cu$), (b) 2 × 2 × 2 supercell (32 atoms) (c) Al-Cu compound structures, (d) $\prime\prime\theta''$-$Al_3Cu$, $\prime\theta'$- and $\theta$-$Al_2Cu$ phases. Earlier computed formation energy of LDA [9] and of GGA-PBE [20] indicated by black and orange empty diamond and upward triangle symbols plotted against the formation energy of compounds and phases obtained in this work before (empty circles) and after including Coulomb repulsion (filled circles), using GGA-PBE + U (U = 4 eV) approach.

configurations up to the formation of $\theta''\theta''$-$Al_3Cu$ using 2 × 2 × 2 supercell (32 atoms)(Fig. 4b), of Al-Cu compound structures (Fig. 4c), and finally of $\theta''\theta''$-$Al_3Cu$, $\theta'\theta'$- and $\theta$-$Al_2Cu$ phases (Fig. 4d). Earlier computed formation energies of LDA [9] and GGA-PBE [20] indicated by black and orange empty diamond and upward triangle symbols

plotted against the formation energy of compounds and phases obtained in this work before (empty circles) and after including Coulomb repulsion (filled circles), using GGA-PBE + U (U = 4 eV) approach.

### 3.2. Lattice parameters of Al-Cu structures

In this section, we discuss the lattice parameter change induced by Cu solute up to the formation of $\theta''$-$Al_3Cu$ and the Al-Cu phases from both DFT-GGA and GGA + U approaches. The lattice parameters of the studied GPZ structures decrease monotonically with Cu atomic fraction with much extensive slope for $c$ parameter, as shown in Fig. 5. The values for $a$ and $c$ parameter linearly fitted as (0.40417 – 0.027089$x$), and (0.40417 – 0.0[illegible]$x$) for 2 × 2 × 2 cell (32 atoms) and (0.40448 – 0.028095$x$) and (0.40448 – 0.094519$x$) for 2 × 2 × 3 cell (48 atoms), where the predicted $c$ parameter for $\theta''$-$Al_3Cu$ is in agreement with the reported experimental value [27]. A large uniaxial strain along $c$ direction has occurred, and subsequently, an increase of the elastic strain energy took place (Fig. 6). This was in agreement with GPZs observed in the experiment, where a strong lattice deformation was taken place into the direction perpendicular to the precipitate layers [28]. Table 1 summarizes the used computational methods to compute known phases, with their corresponding space groups, fully relaxed $a$ and $c$ lattice parameters. Experimental data (Expt.) [27,28] are also included for comparison. We found good agreement with experimental values is derived from PBE + U (U = 4 eV) and PBE standard approaches for all the three phases. For $\theta''$-$Al_3Cu$ phase, very close values of $c$ parameters to the experimental were obtained with a margin of + 0.1% deviation error for PBE, and PBE + U approaches. The $a$ parameter was underestimated by 2%. LDA + U approach underestimates the $a$ parameter of $\theta''$-$Al_3Cu$ phase by ~ 4% and [illegible]rameter by ~ 2%. A similar result was obtained from LDA plain [illegible]ch. For $\theta'$-$Al_2Cu$ phase, identical $c$ parameter values to those m[illegible]d in the experiment were obtained from PBE + U and PBE. The $a$ parameter is overestimated by 1%. LDA and LDA + U underestimate the $c$ parameter similarly by about 2% and $a$ parameter by ~1%, respectively. Finally, for $\theta$-$Al_2Cu$ phase identical $a$ and $c$ parameter values to the experimental were obtained from PBE, and PBE + U approaches, and an underestimation by about 2% was obtained from LDA + U for both lattice parameters. No large deviations were captured from the LDA plain approach for both $a$ and $c$ lattice parameters of $\theta$-$Al_2Cu$ phase. Overall, the best results were obtained by PBE + U (U = 4 eV) and PBE standard approaches, which give these two approaches a great advantage in this study. It is important to mention that obtaining a more accurate lattice parameter requires testing different U values for each lattice parameter, which will increase the computational cost. In the present work, the lattice parameters obtained using U = 4 eV for the known phases in the Al-Cu system are satisfactory and within optimal computational cost and time.

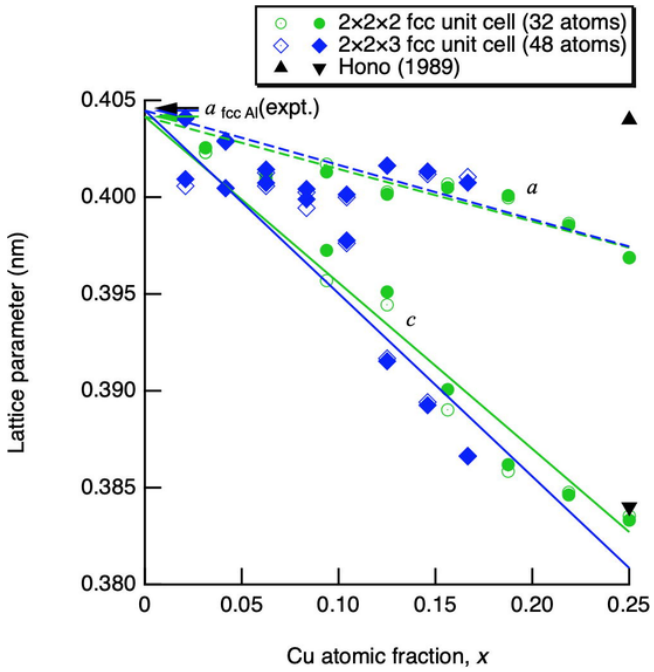


**Fig. 5.** Lattice parameter of Al-Cu GPZs as a function of Cu atomic fraction, $x$, derived from both 2 × 2 × 2 fcc unit cell (32 atoms) and 2 × 2 × 3 fcc unit cell (48 atoms). Empty (filled) symbols are the results of standard DFT method (DFT + U method, U = 4 eV). The experimenat lattice parameter of the fcc Al [26], and of $\theta''$-$Al_3Cu$ [27] are plotted for comparison.

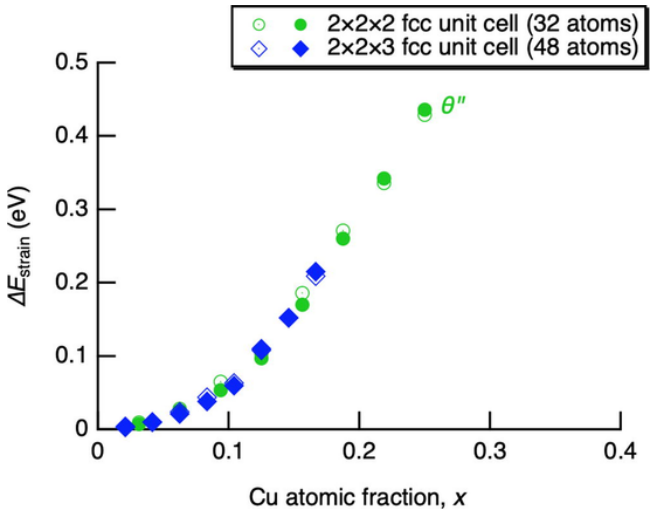


**Fig. 6.** The elastic strain energy induced by Al-Cu GPZs as a function of Cu atomic fraction. Adopted symbols are as in Fig. 5. Previously reported calculation method of the el[illegible]strain energy for tetragonal crystal was adopted [29], and elastic contant s[illegible]ss $C_{ij}$ of $\theta''$-$Al_3Cu$ were used [20].

### 3.3. Advantages of DFT + U and comparison with early studies

A previous study [9] has focused on the formation energy Al-Cu compounds using layered Al-Cu supercells. The weak Cu-Cu layer interaction has hampered a conclusive analysis of the physical precipitate nucleation in Al-Cu system. In this work, instead of considering different Al-Cu layered supercell, we considered the 2-dimensional (2D) clustering and growth of Cu layers along (1 0 0). The models help to establish a better understanding of Cu precipitate nucleation. Indeed, the nucleation of the Cu precipitates showed a continuous process up to $\theta''$-$Al_3Cu$ formation favoring Cu-Cu nearest-neighbor interactions (Fig. 3c). To help the reader reconstructing the configurations, Table 2 illustrates the different lowest energy structures, the number of Cu atoms substituted for Al atoms, and their corresponding sites in fraction coordinates.

The results of 2 × 2 × 2 supercell of Fig. 4b show the beginning of the Cu clustering and the growth of Cu layers along {1 0 0} up to the formation of $\theta''$-$Al_3Cu$ phase, which has the typical structure of three Al layers in between full-formed Cu layers. In an experimental investigation of GPI zones in Al-1.54at.%Cu, high-resolution electron microscopy images revealed information of GPI monolayer growth to GPII ($\theta''$-$Al_3Cu$) through an intermediate stage [31]. Our present model covers this process. Fig. 4c also shows the recomputed Al-Cu compound structures, compared to those reported by others [9,20], the formation energy of Cu single monolayer despite showing a plausible formation mechanism through a flat curve as a function of Cu atomic fraction, it highlights the weak Cu-Cu layer interactions rather than Cu precipitate nucleation. The high energies of $Al_4Cu_2$, $Al_6Cu_2$,

**Table 1**
Summary of the used computational methods, space groups, $a$ and $c$ lattice parameters for known phases in Al-Cu system. Experimental data (Expt.) are also included for comparison. We also list, in parentheses, the deviations of the theoretical values from the corresponding experimental data, $\Delta = (d_{calc.} - d_{exp.})/d_{exp.} \times 100\%$, where $d_{calc.}$ is the calculated data and $d_{exp.}$ the experimental value.

| Method | | Phase | Space group | $a$ (nm) / Δ(%) | $c$ (nm) / Δ(%) | Ref. |
|---|---|---|---|---|---|---|
| Theory (This work) | GGA-PBE + U | $\theta''$-$Al_3Cu$ | *P4/mmm* | 0.396 (–2.0) | 0.769 (+0.1) | |
| | | $\theta'$-$Al_2Cu$ | *I-4m2* | 0.408 (+1.0) | 0.580 (0) | |
| | | $\theta$-$Al_2Cu$ | *I4/mcm* | 0.606 (–1.6) | 0.487 (–0.2) | |
| | GGA-PBE | $\theta''$-$Al_3Cu$ | *P4/mmm* | 0.396 (–2.0) | 0.769 (+0.1) | |
| | | $\theta'$-$Al_2Cu$ | *I-4m2* | 0.408 (+1.0) | 0.580 (0) | |
| | | $\theta$-$Al_2Cu$ | *I4/mcm* | 0.606 (–0.2) | 0.488(0) | |
| | LDA + U | $\theta''$-$Al_3Cu$ | *P4/mmm* | 0.389 (–3.7) | 0.753 (–1.9) | |
| | | $\theta'$-$Al_2Cu$ | *I-4m2* | 0.401 (–0.7) | 0.568 (–2.1) | |
| | | $\theta$-$Al_2Cu$ | *I4/mcm* | 0.594 (–2.1) | 0.477 (–2.3) | |
| | LDA | $\theta''$-$Al_3Cu$ | *P4/mmm* | 0.389 (–3.7) | 0.754 (–1.8) | |
| | | $\theta'$-$Al_2Cu$ | *I-4m2* | 0.401 (–0.7) | 0.569 (–1.9) | |
| | | $\theta$-$Al_2Cu$ | *I4/mcm* | 0.606 (–0.2) | 0.488 (0) | |
| (Other refs.) | LDA-PP-US | $\theta''$-$Al_3Cu$ | *P4/mmm* | 0.387 (–4.2) | 0.773 (+0.7) | [9] |
| | | $\theta'$-$Al_2Cu$ | *I-4m2* | 0.568 (+40.6) | - | |
| | | $\theta$-$Al_2Cu$ | *I4/mcm* | 0.592 (–2.5) | 0.486 (–0.4) | |
| | GGA-PBE | $\theta''$-$Al_3Cu$ | *P4/mmm* | 0.397 (–1.7) | 0.767 (–0.1) | [20] |
| | | $\theta'$-$Al_2Cu$ | *I-4m2* | 0.409 (+1.2) | 0.578 (–0.3) | |
| | | $\theta$-$Al_2Cu$ | *I4/mcm* | 0.605 (–0.3) | 0.488 (0) | |
| Expt. | | $\theta''$-$Al_3Cu$ | *P4/mmm* | 0.404 | 0.768 | [27] |
| | | $\theta'$-$Al_2Cu$ | *I-4m2* | 0.404 | 0.580 | [30] |
| | | $\theta$-$Al_2Cu$ | *I4/mcm* | 0.607 | 0.488 | [30] |

**Table 2**
Illustration of the different lowest energy stable structures, number of Cu atoms, and their corresponding sites in fraction coordinates.

| Structure | Number of Cu atoms | Sites (fraction coordinates) |
|---|---|---|
| *Al-Cu compounds* | | |
| $Al_{13}Cu$ | 2 | (0,0,0.857), (0.5,0.5,0.857) |
| $Al_{11}Cu$ | 2 | (0,0,0.833), (0.5,0.5,0.833) |
| $Al_9Cu$ | 2 | (0,0,0.8), (0.5,0.5,0.8) |
| $Al_7Cu$ | 2 | (0,0,0.75), (0.5,0.5,0.75) |
| $Al_5Cu$ | 2 | (0,0,0.666), (0.5,0.5,0.666) |
| $Al_4Cu_2$ | 4 | (0,0,0.678), (0,0.5,0.821), (0.5,0,0.821), (0.5,0.5,0.678) |
| $Al_6Cu_2$ | 4 | (0,0,0.759), (0,0.5,0.865), (0.5,0,0.865), (0.5,0.5,0.759) |
| $Al_8Cu_2$ | 4 | (0,0,0.808), (0,0.5,0.891), (0.5,0,0.891), (0.5,0.5,0.808) |
| *2 × 2 × 2 fcc unit cell* | | |
| $Al_{31}Cu$ | 1 | (0,0,0) |
| $Al_{30}Cu_2$ | 2 | (0,0,0), (0.25,0.25,0) |
| $Al_{29}Cu_3$ | 3 | (0,0,0), (0.25,0.25,0), (0.5,0,0) |
| $Al_{28}Cu_4$ | 4 | (0.25,0.25,0), (0.25,0.75,0), (0,0.5,0), (0.5,0.5,0) |
| $Al_{27}Cu_5$ | 5 | (0.25,0.25,0), (0.25,0.75,0), (0,0.5,0), (0.75,0.25,0), (0.5,0.5,0) |
| $Al_{26}Cu_6$ | 6 | (0,0,0), (0.25,0.25,0), (0,0.5,0), (0.5,0,0), (0.25,0.75,0), (0.5,0.5,0) |
| $Al_{25}Cu_7$ | 7 | (0,0,0), (0.25,0.25,0), (0,0.5,0), (0.5,0,0), (0.25,0.75,0), (0.75,0.25,0), (0.5,0.5,0) |
| $Al_{24}Cu_8$ | 8 | (0,0,0), (0.25,0.25,0), (0,0.5,0), (0.5,0,0), (0.25,0.75,0), (0.75,0.25,0), (0.5,0.5,0), (0.75,0.75,0) |

and $Al_8Cu_2$ compounds show that they are unlikely to occur during precipitation. The results of Fig. 4c and 4d clearly showed slight high energies for Al-Cu GPZ precipitates and Al-Cu compounds derived from the PBE + U approach compared to those reported by the standard DFT method [9,20,32]. By applying this approach, we succeeded to get the groundstate formation energy for the equilibrium $\theta$-$Al_2Cu$ phase.

### 3.4. Free energy of Al-Cu structures

Fig. 7 shows $\Delta G_f$ (meV/atom) of the Al-Cu structures as a function of temperature (K) for the cases of $\theta''$-$Al_3Cu$, $\theta'$-, and $\theta\theta$-$Al_2Cu$ phases. The metastable $\theta''$-$Al_3Cu$ structure has higher energy than

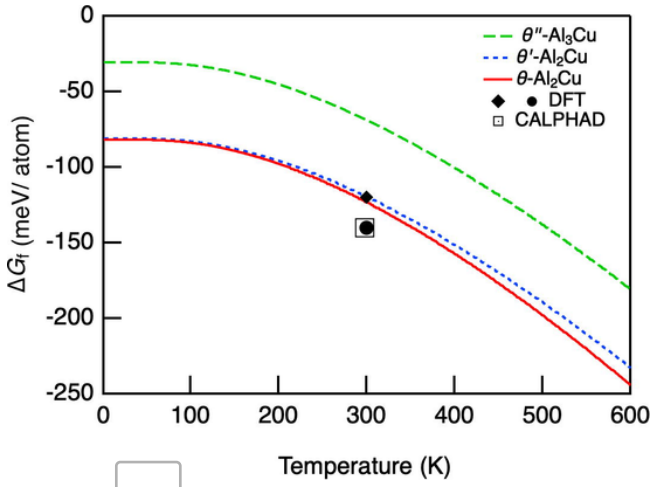


**Fig. 7.** Free energy $\Delta G_f$ (meV/atom), of the Al-Cu structures as a function of temperature (K) for the cases of $\theta''$-$Al_3Cu$, $\theta'$-, and $\theta\theta$-$Al_2Cu$ phases. Values of free energy at $T$ = 300 K from other DFT works (◆, ●) [33,34], and from COST507 CALPHAD database at $T$ = 298 K (⊡)[35], are plotted for comparison.

both $\theta'$-, and $\theta\theta$-$Al_2Cu$ phases, over the whole studied temperature interval. The vibrational free energy contribution causes clear shifts in the formation energy of $\theta'$-, and $\theta\theta$-$Al_2Cu$ phases: Using DFT + U at T = 0 K (Fig. 2), the variation of the formation energy difference between $\theta'$-, and $\theta\theta$-$Al_2Cu$ phases was ~ –3.84 (meV/atom) with U = 4 eV, which is too small to observe in Fig. 7. However, we noticed an apparent increase of the free energy difference between the two phases from ~ T = 0 K, favoring further the stability $\theta\theta$-$Al_2Cu$ phase over $\theta'$-$Al_2Cu$ structure. At higher temperatures, the vibrational excitations cause more preference for the $\theta\theta$-$Al_2Cu$ phase. Here, the vibrational effects already enhance the stability of $\theta\theta$-$Al_2Cu$ as the most stable structure in the Al-Cu system at equilibrium. At 300 K, $\Delta G_f$ = –120 (meV/atom) for $\theta'$-$Al_2Cu$ structure and $\Delta G_f$ = –123 (meV/atom) for $\theta\theta$-$Al_2Cu$ phase. This compares fairly well with –120 meV/atom from previous data reported for the Gibbs free energy of Cu solution in Al at 300 K, derived from LDA and GGA [33], –140 (meV/atom) from [34], and –140 (meV/atom) at 298 K from the COST507

CALPHAD database [35]. The agreement between the calculated $\Delta G_f$ and the experiment validates further our findings.

## 4. Conclusion

To summarise, the relative stabilities of $\theta''$-$Al_3Cu$, $\theta'$- and $\theta$-$Al_2Cu$ structures have been studied using DFT, and DFT + U approaches. Two main findings have been addressed: (1) The importance of the on-site Coulomb repulsion of Cu *3d* states on the energetics and structural properties of Al-Cu compounds through introducing Hubbard term U. (2) The success of the DFT + U approach to estimate the ground state energy of the $\theta$-$Al_2Cu$ phase for U = 4 eV, in agreement with the experimental observations, reported earlier. These results will update the formation energies of the Al-Cu precipitates, which helps get insight into the Cu clustering and formation of Al-Cu intermetallic compounds during heat treatment. Including the vibrational contributions consolidated the relative stability of θ-$Al_2Cu$ phases at elevated temperature. The DFT + U method is expected to accurately estimate the formation energies of other intermetallic phases important in many industrial Al-based alloys, which, in general, will pave the way to better understand their nucleation conditions.

## CRediT authorship contribution statement

**M. Souissi:** Conceptualization, Methodology, Software, Validation, Formal analysis, Investigation, , Visualization, Data curation, Writing - original draft, Writing - review & editing. **C.M. Fang:** Conceptualization, Methodology, Software, Validation, Formal analysis, Investigation, Data curation, Writing - review & editing, Visualization. **R. Sahara:** Conceptualization, Formal analysis, Visualization, Resources, Writing - review & editing. **Z. Fan:** Conceptualization, Supervision, Project administration, Funding acquisition, Resources, Writing - review & editing.

## Declaration of Competing Interest

The authors declare that they have no known competing financial interests or personal relationships that could have appeared to influence the work reported in this paper.

## Acknowledgements

We are grateful for Brunel Center of Advanced Solidification Technology (BCAST), London, United Kingdom (UK), and the Center for Computational Materials Science in the Institute for Materials Research, Tohoku University, Japan for the support and for providing the computational facilities. We thank the Engineering and Physical Sciences Research Council (EPSRC) of the UK and Constellium (UK) for the financial support under the STrain Enhanced Precipitation (STEP) project, in Al-based alloys, registered under the partnership grant number: EP/S036296/1. The authors also thank Prof. Brian Cantor (BCAST), Prof. Isaac Chang (BCAST) and Dr. Chamini Mendis (BCAST) and Dr. Feng Wang (BCAST) for the useful discussions.

Data Availability.

Data will be made available on request.

## References

[1] G.P.M. Leyson, W.A. Curtin, L.G. Hector Jr., C.F. Woodward, Quantitative prediction of solute strengthening in aluminium alloys, Nature Mater. 9 (2010) 750–755, https://doi.org/10.1038/nmat2813.
[2] S.J. Andersen, C.D. Marioara, J. Friis, S. Wenner, R. Holmestad, Precipitates in aluminium alloys, Adv. Phys. X 3 (2018) 791–813, https://doi.org/10.1080/23746149.2018.1479984.
[3] L. Bourgeois, C. Dwyer, M. Weyland, J.-F. Nie, B.C. Muddle, The magic thicknesses of θ′ precipitates in Sn-microalloyed Al–Cu, Acta Mater. 60 (2012) 633–644, https://doi.org/10.1016/j.actamat.2011.10.015.
[4] L. Bourgeois, N.V. Medhekar, A.E. Smith, M. Weyland, J.-F. Nie, C. Dwyer, Efficient atomic-scale kinetics through a complex heterophase interface, Phys. Rev. Lett. 111 (2013) 046102, https://doi.org/10.1103/PhysRevLett.111.046102.
[5] A. Guinier, G.D. Preston, Structure of age-hardened aluminium-copper alloys, Nature 142 (1938) 569–570, https://doi.org/10.1038/142569b0.
[6] D.A. Porter, K.E. Easterling, M.Y. Sherif, Phase Transformations in Metals and Alloys, third ed., Taylor & Francis Group, New York, 2009.
[7] K.F. Kelton, A.L. Greer, Nucleation in Condensed Matter Applications in Materials and Biology, Elsevier, The Netherlands, 2010.
[8] J.W. Martin, Precipitation Hardening, second ed., Oxford, 1998.
[9] S.Q. Wang, M. Schneider, H.Q. Ye, G. Gottstein, First-principles study of the formation of Guinier-Preston zones in Al–Cu alloys, Scripta Mater. 51 (2004) 665–669, https://doi.org/10.1016/j.scriptamat.2004.06.018.
[10] C. Wolverton, V. Ozolins, Entropically favored ordering: The metallurgy of $Al_2Cu$ revisited, Phys. Rev. Lett. 86 (2001) 5518, https://doi.org/10.1103/PhysRevLett.86.5518.
[11] G. Kresse, J. Furthmüller, Efficiency of ab-initio total energy calculations for metals and semiconductors using a plane-wave basis set, Comput. Mater. Sci. 6 (1996) 15–50, https://doi.org/10.1016/0927-0256(96)00008-0.
[12] G. Kresse, D. Joubert, From ultrasoft pseudopotentials to the projector augmented-wave method, Phys. Rev. B 59 (1999) 1758, https://doi.org/10.1103/PhysRevB.59.1758.
[13] J.P. Perdew, K. Burke, M. Ernzerhof, Generalized gradient approximation made simple, Phys. Rev. Lett. 77 (1996) 3865, https://doi.org/10.1103/PhysRevLett.77.3865.
[14] D.S. Sholl, J.A. Steckel, Density Functional Theory: A Practical Introduction, John Wiley & Sons Inc, Hoboken, New Jersey, 2009 https://onlinelibrary.wiley.com/doi/book/10.1002/9780470447710.
[15] A.I. Lichtenstein, V.I. Anisimov, J. Zaanen, Density-functional theory and strong interactions: Orbital ordering in Mott-Hubbard insulators, Phys. Rev. B 52 (1995) R5467, https://doi.org/10.1103/PhysRevB.52.R5467.
[16] N.F. Mott, The basis of the electron theory of metals, with special reference to the transition metals, Proc. Phys. Soc. Section A 62 (1949) 416–422, https://doi.org/10.1088/0370-1298/62/7/303.
[17] J. Hubbard, Electron correlations in narrow energy bands, Proc. R. Soc. A 276 (1963) 238–257, https://doi.org/10.1098/rspa.1963.0204.
[18] C. Toher, J.J. Plata, O. Levy, M. de Jong, M. Asta, M.B. Nardelli, S. Curtarolo, High-throughput computational screening of thermal conductivity, Debye temperarure, and Grüneisen parameter using a quasiharmonic Debye model, Phys. Rev. B 90 (2014) 174107, https://doi.org/10.1103/PhysRevB.90.174107.
[19] D. Ma, B. Grabowski, F. Körmann, J. Neugebauer, D. Raabe, Ab initio thermodynamics of the CoCrFeMnNi high entropy alloy: Importance of entropy contributions beyond the configurational one, Acta Mater. 100 (2015) 90–97, https://doi.org/10.1016/j.actamat.2015.08.050.
[20] Y.F. Ouyang, H.M. Chen, X.M. Tao, F. Gao, Q. Peng, Y. Du, A first-principles study of the structural, mechanical and electronic properties of precipitates of $Al_2Cu$ in Al–Cu alloys, Phys. Chem. Chem. Phys. 20 (2018) 967–976, https://doi.org/10.1039/C7CP06757G.
[21] C.S. Fadley, D.A. Shirley, Electronic Densities of States from X-Ray Photoelectron Spectroscopy, J. Res. National Bureau of Standards Phys. Chem. 74 (4) (1970.6028/jres.074A.045) 10.
[22] M.F. Sunding, K. Hadidi, S. Diplas, O.M. Løvvik, T.E. Norby, A.E. Gunnæs, XPS characterisation of in situ treated lanthanum oxide and hydroxide usingtailored charge referencing and peak fitting procedures, J. Electron Spectrosc. Relat. Phenom. 184 (2011) 399–409, https://doi.org/10.1016/j.elspec.2011.04.002.
[23] G. Panaccione, G. Cautero, M. Cautero, A. Fondacaro, M. Grioni, P. Lacovig, G. Monaco, F. Offi, G. Paolicelli, M. Sacchi, N. Stojić, G. Stefani, R. Tommasini, P. Torelli, High-energy photoemission in silver: Resolving d and sp contributions in valence band spectra, J. Phys. Condens. Matter 17 (2005) 2671–2679, https://doi.org/10.1088/0953-8984/17/17/015.
[24] L. Wang, T. Maxisch, G. Ceder, Oxidation energies of transition metal oxides within the GGA+U framework, Phys. Rev. B 73 (2006) 195107, https://doi.org/10.1103/PhysRevB.73.195107.
[25] J.L. Murray, The aluminium-copper system, Int. Met. Rev. 30 (1985) 211–234, https://doi.org/10.1179/imtr.1985.30.1.211.
[26] W.P. Davey, Precision measurements of the lattice constants of twelve common metals, Phys. Rev. 25 (1925) 753, https://doi.org/10.1103/PhysRev.25.753.
[27] K. Hono, T. Sakurai, H.W. Pickering, Atom-probe analysis of GP zones in an Al-1.7 At. pct Cu alloy, Metall. Trans. A 20A (1989) 1585–1591, https://doi.org/10.1007/BF02663192.
[28] V. Gerold, On the structures of Guinier-Preston zones in Al-Cu alloys, Scripta Metall. 22 (1988) 927–932, https://doi.org/10.1016/S0036-9748(88)80077-2.
[29] M. Souissi, H. Numakura, Elastic properties of Fe–C and Fe–N martensites, ISIJ Inter. 55 (2015) 1512–1521, https://doi.org/10.2355/isijinternational.55.1512.
[30] S. Wang, C. Fan, Crystal structures of $Al_2Cu$ revisited: Understanding existing phases and exploring other potential phases, Metals 9 (2019) 1037, https://doi.org/10.3390/met9101037.
[31] M. Karlík, A. Bigot, B. Jouffrey, P. Auger, S. Belliot, HREM,FIM and tomographic atom probe investigation of Guinier-Preston zones in an Al–1.54 at% Cu alloy, Ultramicroscopy 98 (2004) 219–230, https://doi.org/10.1016/j.ultramic.2003.08.015.
[32] H. Liu, I. Papadimitriou, F.X. Lin, J. LLorca, Precipitation during high

temperature aging of Al–Cu alloys: A multiscale analysis based on first principles calculations, Acta Mater. 167 (2019) 121–135, https://doi.org/10.1016/j.actamat.2019.01.024.

[33] C. Wolverton, V. Ozoliņš, First-principles aluminum database: Energetics of binary Al alloys and compounds, Phys. Rev. B 73 (2006) 144104, https://doi.org/10.1103/PhysRevB.73.144104.

[34] A.Y. Stroev, O.I. Gorbatov, Y.N. Gornostyrev, P.A. Korzhavyi, Solid solution decomposition and Guinier-Preston zone formation in Al-Cu alloys: A kinetic theory with anisotropic interactions, Phys. Rev. Mater. 2 (2018) 033603, https://doi.org/10.1103/PhysRevMaterials.2.033603.

[35] COST507: Thermodynamic Database for Light Metal Alloys, Vol. 2, edited by I. Ansara, A. T. Dinsdale, and M. H. Rand (European Commission, Brussels, 1998). http://www.opencalphad.com/databases/CGNA18499ENC_001.pdf.